Transcriptional regulation of effector-triggered immunity (ETI) in plants: from tissue to cells

Chhillar, H.

Chapter 4
Uncoupling hypersensitive cell death response and disease resistance activated by effector-triggered immunity

Himanshu Chhillar[1], Henk-jan Schoonbeek[2,3], Bruno Pok Man Ngou[3,4,5], Jonathan DG Jones[3,4], Pingtao Ding[1*]

[1]Institute of Biology Leiden, Leiden University, 2333 BE Leiden, The Netherlands
[2]John Innes Centre, Norwich Research Park, Colney Lane, NR4 7UH Norwich, UK
[3] University of East Anglia, Norwich Research Park, NR4 7TJ Norwich, UK
[4] The Sainsbury Laboratory, Norwich Research Park, Colney Lane, NR4 7UH Norwich, UK
[5]Current address: RIKEN Center for Sustainable Resource Science (CSRS), Kanagawa, 230-0045 Yokohama, Japan

This chapter is published in: bioRxiv (2025) October. doi: https://doi.org/10.1101/2025.10.22.683861 and is currently under review.

Abstract

Effector-triggered immunity (ETI) is a major defense strategy in plants and is frequently associated with the hypersensitive response (HR), a localized form of programmed cell death long assumed to be essential for pathogen resistance. However, the causal relationship between HR and effective immunity remains unresolved. We show that the *Arabidopsis cbp60g sard1* double mutant exhibits exaggerated ETI-associated HR but only partial resistance to bacterial and oomycete pathogens, thereby genetically uncoupling cell death from disease resistance without any visible pleiotropic defects. Genome-wide transcriptome profiling reveals that the absence of CBP60g and SARD1 disrupts the balance between immune activators and suppressors, including reduced induction of the Nudix hydrolase NUDT7. Overexpression of *NUDT7* diminishes but does not abolish the heightened HR phenotype in *cbp60g sard1* mutant, indicating that multiple negative regulators act redundantly to restrain immune-associated cell death. These findings demonstrate that HR is not an obligatory determinant of effective resistance against all pathogens and provide mechanistic insight into how plants coordinate transcriptional networks to balance pathogen defense with the containment of host cell death. By refining the relationship between HR and immunity, this work challenges a long-standing paradigm in plant biology and advances our understanding of immune regulation.

Key words

Hypersensitive response (HR), effector-triggered immunity (ETI), master regulators, SA signalling

Introduction

Plants are constantly challenged by diverse pathogens that threaten global crop productivity, causing an estimated 20-40% yield loss annually and over US$220 billion in damages according to the Food and Agriculture

Organization of the United Nations (FAO)[1]. To defend themselves, plants deploy two interconnected layers of innate immunity. Pattern recognition receptors (PRRs) located at the plasma membrane perceive pathogen-associated molecular patterns (PAMPs) to activate pattern-triggered immunity (PTI), while intracellular nucleotide-binding leucine-rich repeat receptors (NLRs) sense pathogen effectors and trigger effector-triggered immunity (ETI)[2]. In *Arabidopsis thaliana* (Arabidopsis), NLRs are classified into coiled-coil (CC)-type (CNLs), Toll/Interleukin-1 receptor/Resistance protein (TIR)-type (TNLs), and RESISTANCE TO POWDERY MILDEW (RPW8)-like CC-type (RNLs) based on their N-terminal domains[3]. Although PTI and ETI share many downstream outputs, including calcium (Ca^{2+}) influx, reactive oxygen species (ROS) production, and large-scale transcriptional reprogramming, ETI responses are typically more robust and sustained[4].

Calcium (Ca^{2+}) signalling is a critical mediator of both PTI and ETI[5]. Ca^{2+} signals are sensed by calcium-binding protein calmodulin (CaM) or/and CaM-like (CML) proteins, which interact with downstream CaM-binding proteins (CBPs) to transduce immune signals[6]. The Arabidopsis CBP60 family is comprised of eight members, seven of which contain canonical Ca^{2+}-dependent CaM-binding domains, whereas SYSTEMIC ACQUIRED RESISTANCE DEFICIENT 1 (SARD1) lacks this domain[7]. Among them, CBP60g and SARD1 are pathogen-inducible transcription factors that promote salicylic acid (SA) biosynthesis by directly activating *ISOCHORISMATE SYNTHASE 1* (*ICS1*) and other defense-associated genes[8–11]. *cbp60g sard1* double mutants lacking both factors CBP60g and SARD1 display reduced SA accumulation, enhanced susceptibility to the bacterial pathogen *Pseudomonas syringae*, and loss of systemic acquired resistance (SAR)[8,12]. Thus, CBP60g and SARD1 have been recognized as central positive regulators of SA-mediated immunity.

A hallmark of ETI is the hypersensitive response (HR), a localized form of programmed cell death that often accompanies disease resistance[13,14]. HR in plants share some morphological features with animal cell death (e.g., cytoplasmic shrinkage, chromatin condensation) but also exhibits plant-specific traits such as vacuolization and chloroplast disruption[15]. While HR and pathogen resistance are often tightly correlated, several genetic studies indicate they can be uncoupled. Early genetic analyses in oat crown rust resistance showed that hypersensitive cell death can be genetically separated from resistance through independent loci, demonstrating that HR is not required for effective disease resistance[16]. Consistent with this principle, analogous uncoupling has been observed in Arabidopsis, where loss of the metacaspase *mc1* drastically reduces HR but does not abolish resistance[17,18], and mutants such as *defense, no death* (*dnd1*), *HR-like lesion mimic 1* (*hlm1*), and *lesion simulating disease resistance 1* (*lsd1*) maintain resistance despite altered or spontaneous cell death[19–21]. However, these Arabidopsis mutants often show pleiotropic effects, complicating interpretation[22].

Here, we identify the *cbp60g sard1* double mutant as a valuable model to dissect the relationship between disease resistance and HR. Unlike other uncoupling mutants, *cbp60g sard1* exhibits enhanced HR in the absence of growth defects, providing a genetically tractable system to separate cell death from resistance. We demonstrate that CBP60g and SARD1 contribute to ETI-mediated resistance mediated by different types of NLRs, while paradoxically restraining ETI-associated HR. In addition, we test their contribution to necrotrophic pathogen interactions to gain a broader understanding of its immune function.

By integrating genome-wide transcriptomic profiling with functional assays, we uncover that CBP60g and SARD1 serve as dual regulators of the immune transcriptome: they promote defense-related gene activation

while simultaneously maintaining negative regulatory circuits, including members of the Nudix hydrolase family (NUDT). Functional analysis of *NUDT7* demonstrates its role in buffering ETI-associated cell death but also reveals that its overexpression cannot fully rescue the enhanced HR of *cbp60g sard1* double mutant. Together, our findings establish CBP60g and SARD1 as master integrators of positive and negative immune regulation and provide mechanistic insight into how plants fine-tune immune output, while decoupling HR from disease resistance.

Results

The *cbp60g sard1* mutant partially compromises ETI-mediated bacterial resistance but does not impair PTI

To assess the role of CBP60g and SARD1 in effector-triggered immunity (ETI), we challenged the *cbp60g sard1* (*gh* thereafter) double mutant with *Pseudomonas syringae* pv. *tomato* DC3000 strains carrying either AvrRps4 or AvrRpt2, alongside the corresponding empty vector (EV) controls. In wild-type (WT) Col-0, both effectors conferred strong resistance compared with EV infections, whereas *gh* plants showed only partial restriction of bacterial growth (**Figure 1A, S1A**), in consistence with previous studies[8,9]. AvrRps4 is recognized by the Toll/Interleukin-1 receptor/Resistance protein (TIR)-type nucleotide-binding leucine-rich-repeat receptors (NLRs) (or TNLs) RESISTANCE TO RASTONIA SOLANACEARUM 1 (RRS1)/RESISTANCE TO PSEUDOMONAS SYRINGAE 4 (RPS4) and RRS1B/RPS4B[23,24], and AvrRpt2 is recognized by the Coiled-coil (CC)-type NLR (or CNL) RPS2[25,26]. Therefore, the observed reduction of immunity in *gh* was comparable across TNL- and CNL-triggered pathways, indicating CBP60g and SARD1 contribute broadly to PTI+ETI-mediated defense. However, resistance was not completely abolished, suggesting residual immune signalling through

salicylic acid (SA), N-hydroxy pipecolic acid (NHP), or additional regulatory modules[27].

In contrast, when infected with the non-pathogenic strain DC3000 hrcC$^-$, which activated pattern-triggered immunity (PTI) but lacks a type-III secretion system, *gh* mutant supported bacterial growth at levels similar to WT Col-0 (**Figure 1B**). Consistently, *gh* plants displayed WT-like flg22-induced reactive oxygen species (ROS) bursts (**Figure S1B, S1C**). These results indicate that the absence of CBP60g and SARD1 are not sufficient to compromise canonical PTI signalling outputs but instead play a more specific and central role in PTI+ETI.

Together, these findings establish that CBP60g and SARD1 are broadly required for full ETI-mediated resistance across distinct NLR classes, while their absence leaves PTI early signaling intact. The partial loss of ETI in *gh* mutants highlights both the robustness of immune signalling and the presence of compensatory pathways that operate in parallel to CBP60g and SARD1.

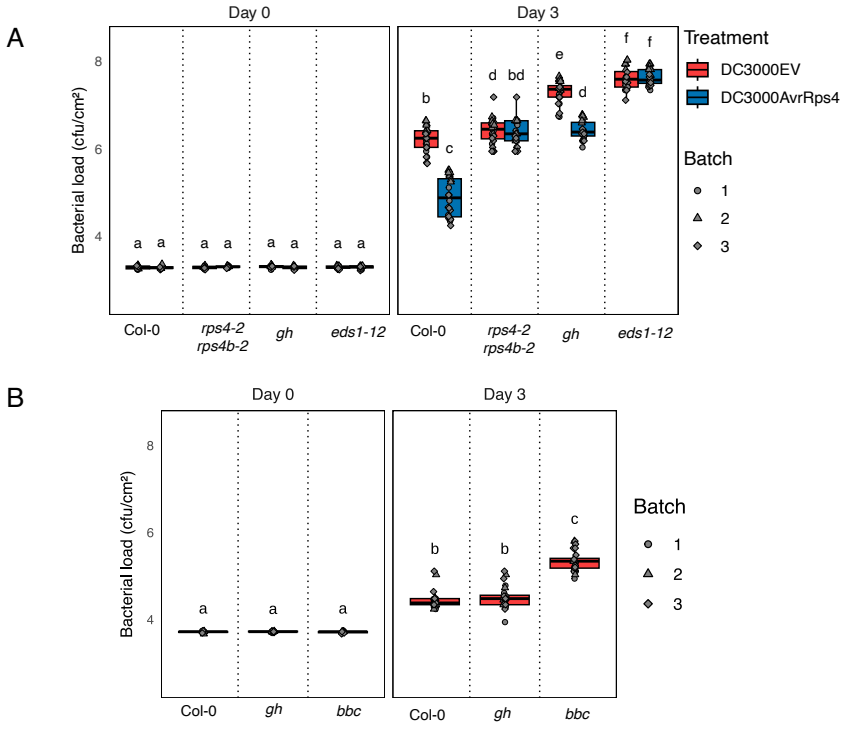

Figure 1. Contribution of CBP60g and SARD1 in PTI and ETI. A. Leaves of Col-0, *resistant to p. syringae* (*rps4-2 rps4b-2*), *enhanced disease susceptibility 1* (*eds1-12*) and *cbp60g sard1* (*gh*) were infiltrated with *Pseudomonas syringae* pv. *tomato* DC3000 carrying either an empty vector (EV) or AvrRps4. Bacterial growth was quantified as colony-forming units (CFU) at 0- and 3-days post-inoculation (dpi). Statistical differences are indicated by different letters (Tukey's honestly significant difference [HSD] test, $p \leq 0.05$). B. Col-0, *gh* (*cbp60g sard1*), and *bbc* (*bak1-5, bkk1-1, and cerk1*) plants were infiltrated with DC3000 *hrcC*$^{-}$, and bacterial titres were measured at 0 and 3 dpi. Statistical differences are denoted by different letters (Tukey's HSD test, $p \leq 0.05$).

The *sard1 cbp60g* mutant enhances ETI-induced hypersensitive cell death

The hypersensitive response (HR) is a hallmark of effector-triggered immunity (ETI), so we examined whether CBP60g and SARD1 contribute

to the regulation of ETI-associated cell death. When infiltrated with *Pseudomonas fluorescence* (Pf0-1 'EtHAn' strains) expressing AvrRps4 or AvrRpt2[28,29], *gh* mutants showed markedly stronger macroscopic HR symptoms compared with WT Col-0 (**Figure 2A**). This phenotype was corroborated by electrolyte leakage assays, which revealed significantly elevated ion leakage in *gh* relative to WT following both TNL- and CNL-mediated (AvrRps4 and AvrRpt2, respectively) recognition (**Figure 2B-D, S2A, S2B**). Enhanced HR in *gh* was evident as early as 4 hours post infiltration (hpi) and was much pronounced at 22 hpi in Col-0 or other control genotypes. These results indicate that CBP60g and SARD1 normally act to limit the amplitude of ETI-associated cell death across distinct NLR classes.

To exclude potential contributions of pattern-triggered immunity (PTI), we analysed HR phenotype in inducible ETI systems[30]. When crossed into estradiol-inducible AvrRps4 (the Super ETI or SETI line) or AvrRpt2 plants[30,31], *gh* mutants exhibited enhanced cell death upon ETI induction but not under mock conditions (**Figure 2C-E, S3A, S3B**). Moreover, when PTI and ETI were activated separately or in combination (PTI+ETI), SETI_*gh* displayed stronger cell death under both ETI and PTI+ETI compared with SETI_WT, while PTI alone induced no such enhancement (**Figure S3C**).

Thus, despite reduced pathogen resistance, *gh* plants paradoxically undergo more severe ETI-associated HR. This genetic separation of cell death from disease resistance highlights the distinct regulatory layers governing immune outputs and positions the *gh* mutant as a powerful model for dissecting how plants balance defense activation with the containment of self-damaging responses.

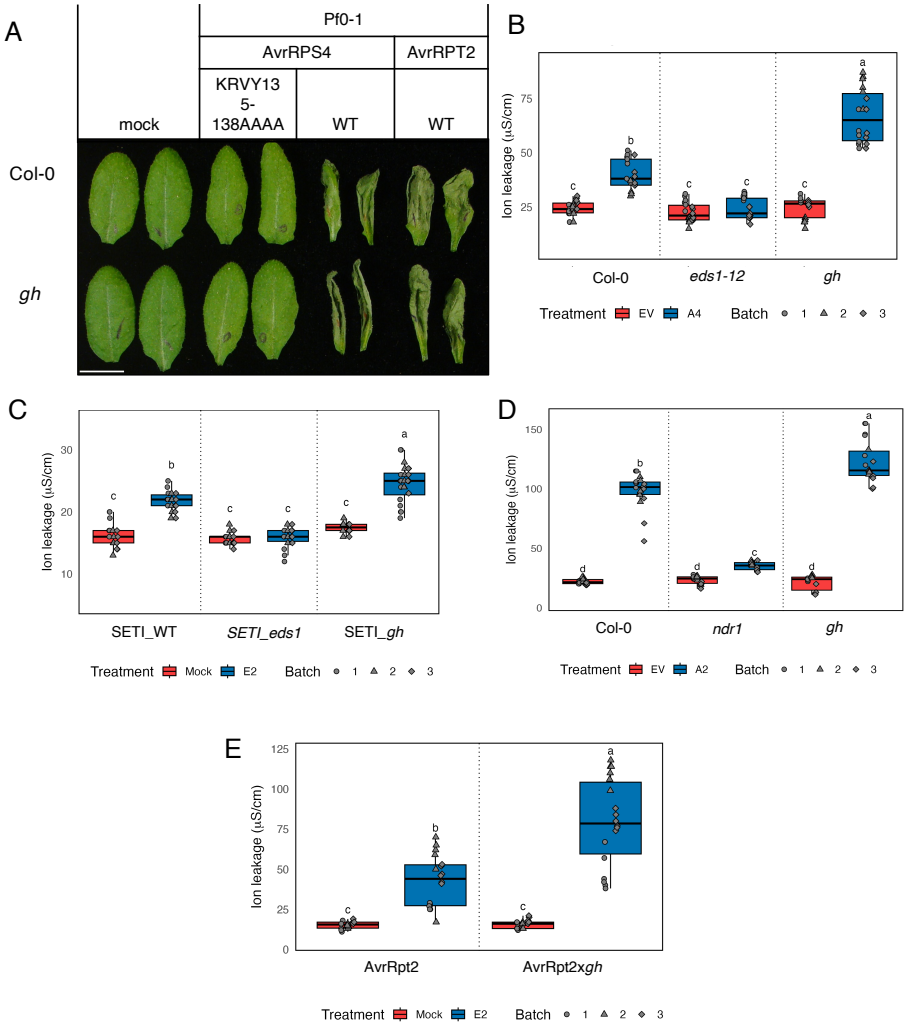

Figure 2. Role of CBP60g and SARD1 in ETI-enhanced HR. A. Leaves of the indicated genotypes were infiltrated with Pf0-1 strains expressing AvrRps4 ^{WT}, AvrRps4 $^{KRVY135–138AAAA}$, or AvrRpt2 and imaged at 1-day post-infiltration (dpi). Scale bar = 1 cm. B, C. Ion leakage assays were performed in Col-0, *enhanced disease susceptibility 1* (*eds1-12*), and *cbp60g sard1* (*gh*) infiltrated with Pf0-1 carrying an empty vector (EV) or AvrRps4 (A4) (B). Ion leakage was also measured in SETI_WT, SETI_*enhanced disease susceptibility 1* (SETI_*eds1*), and SETI_*gh* infiltrated with mock or estradiol (E2) treatment. C. Measurements

were taken 3dpi. D, E. Ion leakage assays were performed in Col-0, *non-race-specific disease resistance 1* (*ndr1*), and *gh* infiltrated with Pf0-1 carrying empty vector or AvrRpt2 (D). Ion leakage was also measured in estradiol (E2) inducible AvrRpt2 and Avrrpt2x*gh* infiltrated with mock or estradiol (E2). E. Measurements were taken 24h post-infiltration. Different letters indicate statistically significant differences (Tukey's HSD test, $p \leq 0.05$).

The *sard1 cbp60g* mutant does not enhance susceptibility to necrotrophic fungi

Necrotrophic pathogens exploit host cell death to promote infection[32,33]. Given the enhanced HR in *gh* mutants, we tested whether this would render plants more vulnerable to the necrotrophic fungus *Botrytis cinerea*. Unexpectedly, *gh* plants displayed lesion sizes comparable to WT Col-0 **(Figure 3).**

In contrast, eds5 mutants, an established SA-deficient background, showed significantly larger lesions, consistent with their increased susceptibility to *B. cinerea* (**Figure 3**). Previous work demonstrated that SA-deficient mutants, including *eds5*, undergo enhanced ETI-associated cell death and ion leakage in response to effectors such as AvrRpt2[34], which correlates with increased vulnerability to necrotrophs. Based on this precedent, we expected *gh* mutants to mirror this phenotype. Instead, *gh* mutants retained WT-like resistance to *B. cinerea* despite their stronger HR.

These findings reveal that enhanced HR in *gh* does not translate into increased susceptibility to necrotrophs, in contrast to SA-deficient backgrounds. This suggests that the cell death program in *gh* is qualitatively distinct, potentially representing a regulated immune-associated pathway that is uncoupled from the necrotrophy-promoted cell death observed in *eds5* and similar mutants.

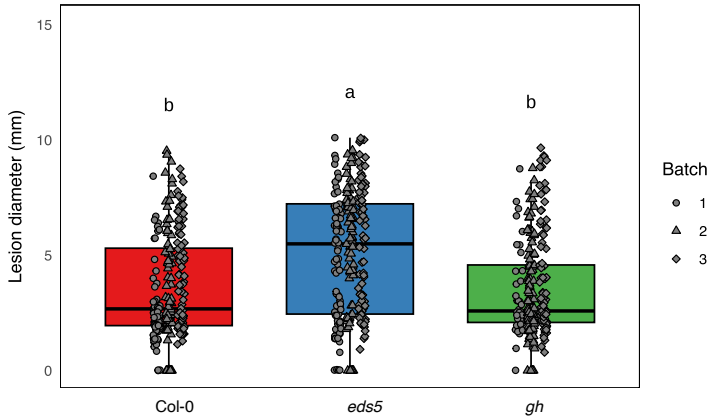

Figure 3. CBP60g and SARD1 do not contribute to resistance against the necrotrophic pathogen *Botrytis cinerea*. The indicated genotypes of Col-0, *enhanced disease susceptibility* 5 (*eds5*) and *cbp60g sard1* (*gh*) were droplet-inoculated with *B. cinerea* B05.10, and lesion diameter were measured 72-96 h post-inoculation. Different letters denote statistically significant differences (Tukey's HSD test, $p \leq 0.05$).

The *sard1 cbp60g* mutant disrupts early transcriptional responses to ETI

Early response genes (ERGs)[35,36] are rapidly induced downstream of both pattern-recognition receptors and NLRs, and many are downregulated in the *gh* double mutant. To dissect the transcriptional programs controlled by CBP60g and SARD1, we performed RNA-seq on Col-0 and *gh* plants challenged with Pf0-1 EtHAn:AvrRps4^{KRVYmutant} (PTI) and Pf0-1EtHAn:AvrRps4^{WT} (PTI+ETI)[37].

Across all conditions, we detected 12,174 differentially expressed genes (DEGs, FDR < 0.01, |$\log_2$ fold change| ≥ 1) (**Figure 4**). Hierarchical clustering grouped these DEGs into 10 major clusters (**Figure 4A**), highlighting widespread reprogramming of the immune transcriptome upon the loss of CBP60g and SARD1.

Cluster 5 was particularly notable: genes in this group were strongly induced during PTI and PTI+ETI in Col-0 but showed markedly attenuated expression in *gh* (**Figure 4**). Gene Ontology (GO) analysis revealed enrichment for defense and metabolic pathways (**Figure 5A**), including salicylic acid (SA) biosynthesis (*ICS1* and *PBS3*), N-hydroxypipecolic acid (NHP) biosynthesis (*ALD1*, *SARD4* and *FMO1*), the hypersensitive response (HR), and core immune regulators (*EDS1* and *PAD4*). Transcription factors from immunity associated families (WRKYs, ERFs and NACs) were also prominent, indicating a broad defect in immune reprogramming in the *gh* mutant.

Cluster 8 showed a similar loss of induction in *gh* and was enriched for hormone- and metabolism-related genes (**Figure 5B**), including pathways linked to ethylene (ET), jasmonic acid (JA), and abscisic acid (ABA). These data suggest that CBP60g and SARD1 not only control canonical immune regulators but also orchestrate the metabolic adjustments that accompany immune activation.

Together, these findings establish CBP60g and SARD1 as central integrators of ETI-induced transcription with some involvement in PTI-induced transcription. Their absence compromises the activation of both immune signalling and metabolic pathways, highlighting their dual role in coordinating transcriptional and physiological reprogramming during plant immunity.

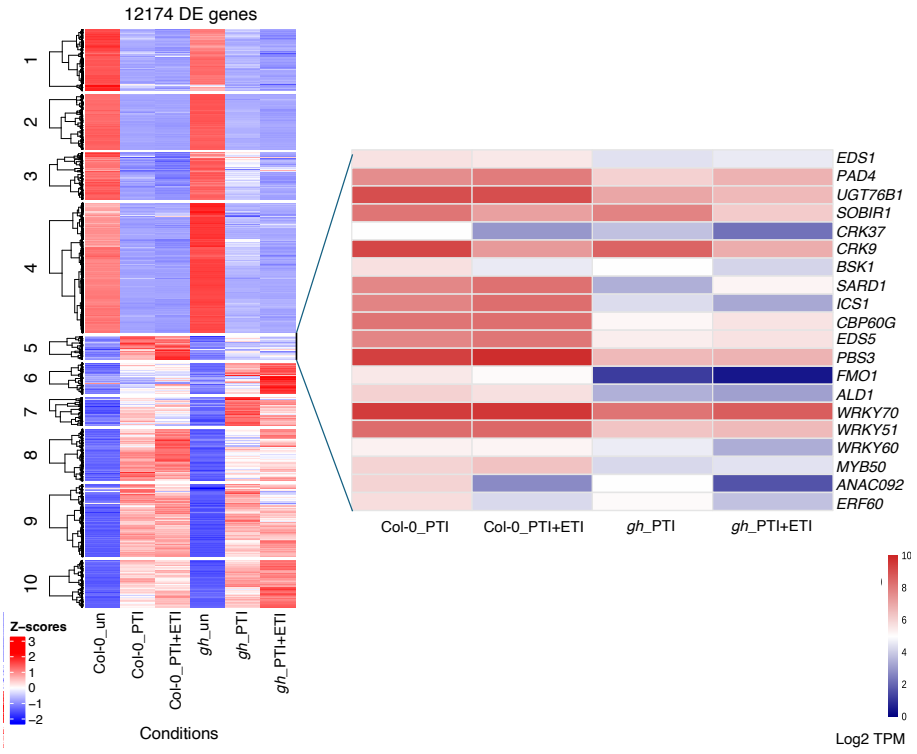

Figure 4. CBP60g/SARD1-dependent transcriptional changes during immune activation. Five- to six-week-old Col-0 and *cbp60g sard1* (*gh*) mutant plants were infiltrated with Pf0-1 carrying either an empty vector or AvrRps4. Leaf samples were collected 4 h post infiltration (hpi) for RNA-seq analysis. The left heatmap shows normalized expression (Z-score) of differentially expressed genes (false discovery rate [FDR] < 0.01; log2 fold change ≥ 1). The right heatmap highlights expression patterns of key immune genes from cluster 5 which showed compromised expression in *gh* mutants following immune activation.

Dual regulatory roles of CBP60g and SARD1 in the plant immune transcriptome

In addition to their well-established roles as positive regulators of immunity, our transcriptome-scale analysis revealed that CBP60g and SARD1 also exert negative regulatory control over specific gene modules.

Hierarchical clustering identified clusters 6 and 10, which contained genes upregulated in the *gh* mutant compared with Col-0, suggesting these genes are normally constrained by CBP60g and SARD1 (**Figure S4A, S4B, Table 1**). GO enrichment associated these clusters with defense responses, calcium signalling, cell death, and cellular organization, indicating that CBP60g and SARD1 help prevent widespread mis-regulation of physiological and cellular processes.

Importantly, these functions link CBP60g and SARD1 to the control of immune intensity and spatial localization. By repressing signalling modules closely tied to programmed cell death, CBP60g and SARD1 may prevent excessive or ectopic immune activation that could be detrimental to the host. Expression analysis further showed that several well-characterized negative regulators, including members of the Nudix hydrolase family (*NUDTs*), *BON1 ASSOCIATED PROTEIN 1* (*BAP1*), BONZAI 3 (*BON3*), and *LESION SIMULATING DISEASE 1* (*LSD1*), were significantly reduced in *gh* (**Figure S4C**). While some of these genes were previously identified as CBP60g and SARD1 binding targets[12], our results demonstrate their functional mis-regulation in the mutant background, providing a transcriptome-level view of how CBP60g and SARD1 integrate both positive and negative arms of immune regulation.

Beyond CBP60g and SARD1 dependent pathways, our data also uncovered modules that appear largely independent of these factors. Cluster 9, for instance, was only modestly affected in *gh* (**Figure 4**) and showed minimal overlap with the SARD1 ChIP-seq dataset [12], in contrast to the strong overlap observed for clusters 5 and 8 (**Figure 5C, Table 2**). Motif enrichment of cluster 9 highlighted families such as WRKY, MYB, ANAC, ETHYLENE RESPONSE FACTOR (ERF), BASIC LEUCINE ZIPPER (bZIP), and BASIC-HELIX-LOOP-HELIX (bHLH), with WRKY motifs being the most enriched (**Figure 5D, Table 3**). These findings

indicate that additional transcription factor networks operate in parallel to CBP60g and SARD1 to drive ETI-associated transcriptional reprogramming.

Together, these results support a model in which CBP60g and SARD1 function as master integrators of the immune transcriptome, coordinating both activation and repression of defense programs. At the same time, the persistence of CBP60g and SARD1independent modules underscores a layered regulatory architecture that balances robust defense activation with the containment of self-damaging responses.

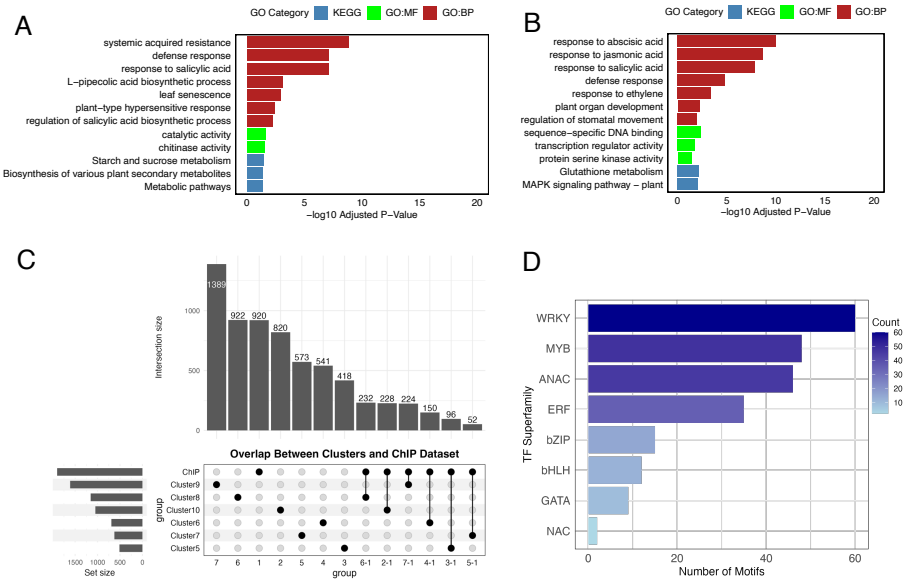

Figure 5. Functional analysis of CBP60g/SARD1-dependent and independent gene clusters.

A-B. Gene Ontology (GO) enrichment analysis of clusters 5 and 8 was performed using g:Profiler. Enriched GO terms are categorized into biological processes (GO:BP), cellular components (GO:KEGG), and molecular functions (GO:MF) (FDR ≤ 0.05, Benjamini–Hochberg correction). C. UpSet plot showing overlap of

differentially expressed genes (DEGs) from various clusters with the SARD1 ChIP-seq dataset reported by Sun et al. (2015). Cluster 9 exhibits minimal overlap with the ChIP-seq dataset. D. Bar graph depicting enrichment of transcription factor motifs in cluster 9 with representation from all major classes such as WRKYs, MYBs, ANACs, ERFs etc.

Overexpressing of *NUDT7* only partially suppresses enhanced ETI-associated HR in *cbp60g sard1* mutants

We hypothesized that the enhanced HR in *gh* plants arises from the misregulation of transcriptional repressors, leading to an imbalance between immune activation and suppression. Previous studies suggested that CBP60g and SARD1 finetune ETI in part by promoting the expression of negative regulators, including members of the Nudix hydrolase family[38]. Nudix hydrolases hydrolyse nucleoside diphosphates linked to other moieties (X), thereby maintaining nucleotide homeostasis and modulating stress responses[39]. This enzymatic activity is conserved across all domains of life, with 29 homologs identified in Arabidopsis (**Figure S4D**), underscoring their central role in cellular regulation.

To explore their contribution to ETI regulation, we profiled Nudix hydrolase family members in responses to Pf0-1 EtHAn:AvrRps4 (**Figure S4D**). Among them, *NUDT7* was the most strongly induced in Col-0 but showed markedly reduced induction in *gh* (**Figure 6A**), indicating that CBP60g and SARD1 are required for ETI-dependent transcriptional activation of this key negative regulator. Earlier findings have also pointed out *NUDT7* as negative regulator of cell death[40–42]. Consistent with these reports, more recently *NUDT7* has been shown to suppress TIR-only protein RESPONSE TO THE BACTERIAL TYPE III EFFECTOR PROTEIN HOPBA1 (RBA1)-mediated cell death in *Nicotiana benthamiana*[43], supporting its conserved role as a negative regulator of immune-associated HR.

To test whether restoring *NUDT7* expression could compensate for the loss of CBP60g and SARD1, we generated *NUDT7* overexpression (*NUDT7*^{OE}) lines in both SETI_WT and SETI_*gh* backgrounds (**Figure S5A**). Upon infiltration with Pf0-1 EtHAn_AvrRps4, *NUDT7*^{OE} plants exhibited reduced HR compared with their non-transgenic counterparts, confirming a suppressive role for *NUDT7* (**Figures 6B, S5B, S5C**). However, in the *gh* background the enhanced HR was only partially suppressed, indicating that *NUDT7* overexpression alone cannot restore immune homeostasis that is caused by the loss of CBP60g and SARD1.

These results demonstrate that although NUDT7 contributes to buffering ETI-associated cell death, the severe HR phenotype in *gh* mutants reflects broader misregulation of multiple negative immune regulators beyond NUDT7. Thus, CBP60g and SARD1 act at the network level to balance immune activation with transcriptional repression, and loss of this dual control cannot be compensated by a single negative regulator.

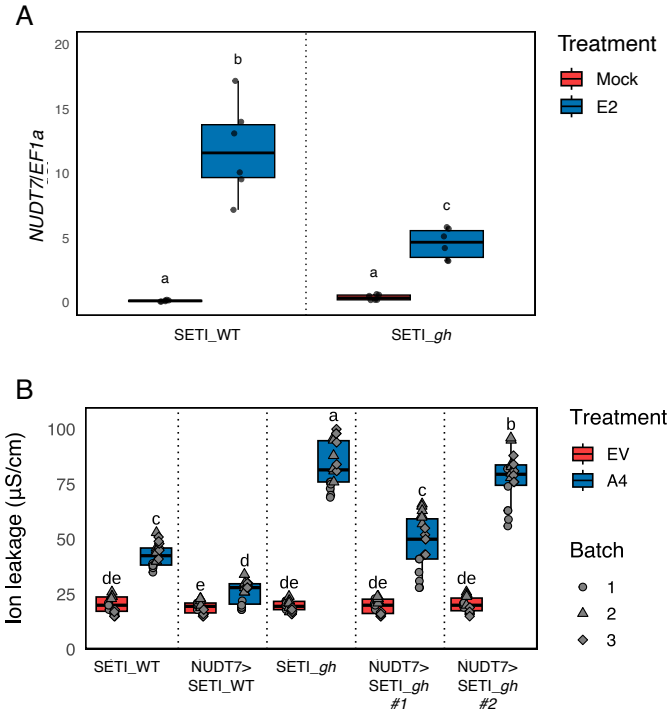

Figure 6. Contribution of NUDT7 to ETI-induced cell death. A. Five-week-old SETI_WT and SETI_*gh* plants were infiltrated with mock or 50 µM estradiol (E2). Samples were collected 4 h post infiltration (hpi) for RNA extraction and qPCR analysis. *NUDT7* expression levels are shown relative to *EF1α*. Different letters indicate significant differences (Tukey's HSD test, $p \leq 0.05$). B. Ion leakage assays of the indicated genotypes infiltrated with Pf0-1 carrying either an empty vector (EV) or AvrRps4 (A4). Measurements were taken 24 hpi. Statistical differences are denoted by different letters (Tukey's HSD test, $p \leq 0.05$).

Discussion

CBP60g and SARD1 are widely recognized as transcriptional activators of plant immunity, acting upstream of SA biosynthesis and systemic signalling. Here, we show that their contribution extends across both TNL- and CNL-mediated ETI, as *cbp60g sard1* (*gh*) double mutants displayed reduced resistance to bacterial carrying AvrRps4 and AvrRpt2. Notably,

while SARD1 directly binds to promoters of *EDS1* and *PAD4*, both of which encode central components of TNL signalling, it does not bind to *NDR1*, encoding the CNL adaptor, and *NDR1* expression is unchanged in *gh* compared to the WT. The observation that both pathways are equally compromised suggests that CBP60g/SARD1 also regulate shared downstream immune modules that act as convergence points between NLR classes, in addition to their established role in SA biosynthesis.

Although CBP60g and SARD1 bind promoters of PTI-associated genes and are transcriptionally induced upon PAMP treatment, *gh* mutants did not exhibit altered resistance against the *hrcC*$^{-}$ mutant, which elicits canonical PTI. These findings argue that CBP60g and SARD1 are not essential for baseline PTI outputs. Instead, they likely function as transcriptional hubs that bridge PTI and ETI, enabling mutual potentiation of these two immune layers. This is consistent with our SETI-based transcriptomic profiling, which indicates that CBP60g and SARD1 control early immune gene reprogramming in an ETI-specific context.

One of the most striking features of the *gh* mutant is its exaggerated hypersensitive response (HR) upon ETI activation, despite reduced resistance. This phenotype sharply contrasts with most previously characterized HR regulators, which often show constitutive defense activation, pleiotropic developmental defects, or spontaneous lesion formation. Unlike *dnd1*, *hlm1*, or *lsd1*, *gh* plants grow normally and lack constitutive immunity, making them a valuable genetic model to uncouple cell death from resistance. Interestingly, while *eds5* mutants (also SA-deficient) exhibit enhanced susceptibility to the necrotrophic pathogen *Botrytis cinerea, gh* plants do not, despite comparable reductions in SA accumulation and enhanced HR[8,44]. This suggests that HR in *gh* is qualitatively distinct from that in other SA-deficient mutants and may not be exploited by necrotrophs.

Transcriptomic profiling revealed that CBP60g and SARD1 exert both positive and negative transcriptional control directly or indirectly. Clusters 5 and 8, strongly induced in Col-0 but attenuated in *gh*, included genes required for SA and NHP biosynthesis (*ICS1, PBS3, ALD1, FMO1, SARD4*), the *EDS1/PAD4* module, and numerous defense-related transcription factors, corresponding closely to known CBP60g and SARD1 binding targets. By contrast, clusters 6 and 10 were upregulated in *gh* and enriched for genes involved in Ca^{2+} signalling, cellular organization, and cell death execution, indicating that CBP60g and SARD1 normally constrain HR-promoting programs. Cluster 9, which was minimally affected in *gh* and showed little overlap with SARD1 ChIP targets, was enriched for WRKY, MYB, ANAC, ERF, bZIP, and bHLH motifs, suggesting CBP60g and SARD1 independent transcriptional programs that sustain residual ETI. Together, these findings support a model in which CBP60g and SARD1 function as dual regulators, promoting defense gene activation while simultaneously restraining runaway cell death, such that their absence both weakens essential defense modules and releases repression on HR-associated pathways, producing the paradoxical phenotype of reduced resistance but enhanced HR.

We further tested this model by examining Nudix hydrolases, a family of nucleotide-metabolizing enzymes implicated in immune homeostasis. Among them, *NUDT7* was strongly induced upon ETI in Col-0 but showed markedly reduced expression in *gh*. Overexpression of *NUDT7* suppressed HR in both WT and *gh* backgrounds, but could not fully restore homeostasis in *gh*, demonstrating that loss of CBP60g and SARD1 disrupts multiple layers of negative regulation. This highlights that immune homeostasis depends on a combinatorial network of repressors, rather than on individual factors alone.

Our results broaden the view of CBP60g and SARD1 from SA-dependent activators to network-level integrators that balance immune activation and suppression. The exaggerated HR yet reduced resistance of *gh* mutants reveal that these two immune outputs, which can be associated in some contexts, can also be genetically and mechanistically separated. Similar uncoupling between hypersensitive cell death and disease resistance has been reported previously. For example, RRS1/RPS4- and RPP1-mediated immunity can confer effective resistance in the absence of AvrRps4-induced HR, and genetic analyses have shown that cell death and resistance can originate from distinct signalling routes downstream of TIR-NLR activation[45]. Consistent with these observations at a broader scale, [46]showed that a majority of ETI-eliciting effectors across the *Pseudomonas syringae* pan-genome trigger effective defense without inducing macroscopic HR, demonstrating that HR is not an obligatory output of ETI in Arabidopsis. Future studies combining high-resolution temporal profiling, network modelling, and metabolomic analyses will be critical to identify upstream signals and downstream executioners of this atypical (independent of resistance) HR. More broadly, the dual roles of CBP60g and SARD1 underscore how plants achieve robust pathogen defense while minimizing self-inflicted damage, a principle of immune regulation with both mechanistic and translational significance.

Acknowledgments

HC and PD acknowledge European Research Council Starting Grant “R-ELEVATION” (grant agreement: 101039824). JDGJ was supported by the Gatsby Charitable Foundation (UK).

Competing interests

The authors declare no competing interests.

Author contributions

PD conceptualized and oversaw the inception of the research project. The experimental work was collaboratively conducted by HC, H-JS, and BPMN. Data analysis and figure generation were performed by HC and PD. JDGJ was involved throughout the project, providing valuable discussions that significantly shaped the research HC and PD wrote the initial manuscript draft. All co-authors contributed to subsequent revisions. The final manuscript was prepared by HC and PD and was approved for submission by all authors.

Data and code availability

- The RNA-seq data for this study have been deposited in the European Nucleotide Archive (ENA) at EMBL-EBI under EMBL-EBI: PRJEB34958.
- All codes are available via GitHub: https://github.com/chhilla/HR_gh

Materials and Methods

Plant material and growth conditions

Arabidopsis thaliana accessions Col-0 and a β-estradiol (E2) inducible Super-ETI line (SETI_WT), were used as the wild-type controls in this study. Mutants of *eds1-2*, eds1-12, *sard1-1 cbp60g-1* that were used in this study have been previously described[8,47,48]. Mutants of *eds1-2* and *sard1-1 cbp60g-1* were crossed with SETI_wt to generate SETI_*eds1-2* and SETI_*gh* plants respectively. NUDT7^{OE} overexpression plants in different genetic backgrounds were generated by transforming *AtRBCS1A::gDNANUDT7*-mEGFP-tHSP18.2 construct generated through In-fusion cloning into the SETI_WT and SETI_*gh* plants. Plants were grown at 21°C under long-day conditions (16 h light, 8 h dark), and at 50% humidity.

Bacterial strains and growth conditions

Pseudomonas syringae pv. tomato (*Pst*) DC3000 EV (carrying empty vector) grown on the King's B medium plates containing 25 μg mL^{-1} rifampicin, and 50 μg mL^{-1} kanamycin and *Pst* DC3000 *hrcC*$^{-}$ were grown on the King's B medium plates containing 25 μg mL^{-1} rifampicin. *Pseudomonas fluorescens* engineered with a Type III secretion system (Pf0-1 'EtHAn' strains) expressing empty vector or AvrRpt2 was grown on the King's B medium plates with 50 μg mL^{-1} kanamycin, 34 μg mL^{-1} Chloramphenicol and 5 μg mL^{-1} tetracycline. *Pseudomonas fluorescens* engineered with a Type III secretion system (Pf0-1 'EtHAn' strains) expressing AvrRps4 was grown on the King's B medium plates with 10 μg mL^{-1} Gentamycin, 34 μg mL^{-1} Chloramphenicol and 5 μg mL^{-1} tetracycline. All the Pseudomonas strains were grown on plates at 28°C for 2 days for further inoculum preparation.

Hypersensitive cell death response phenotyping in Arabidopsis

Pseudomonas fluorescens engineered with a Type III secretion system (Pf0-1 'EtHAn' strains) expressing one of the effectors (AvrRps4 or AvrRpt2), or pVSP61 empty vector were grown on selective KB plates for 24 h at 28 °C[28,36]. Bacteria were harvested from the plates, resuspended in infiltration buffer (10 mM $MgCl_2$), and the concentration was adjusted to OD600=0.2 (108 CFU mL^{-1}). The abaxial surfaces of 5-week-old Arabidopsis leaves were hand infiltrated with a 1 mL needleless syringe. Cell death was monitored 3dpi after infiltration.

Electrolyte leakage assay

Two leaves of 5-week-old *Arabidopsis* plants were hand infiltrated using a 1-mL needleless syringe with 50 μM E2 dissolved in Milli-Q water or Pf0-1 'EtHAn' strain carrying AvrRps4 or AvrRpt2 dissolved in 10mM $MgCl_2$ (OD_{600}=0.2). DMSO in Milli-Q water or 10mM $MgCl_2$ was used as mock treatment. Leaf discs were collected with a 7-mm diameter cork borer from

infiltrated leaves on paper towels. Leaf discs were dried and transferred into 2 mL of deionised water in 12-well plates (2 leaf disks per well. The plate was incubated for 30 min in a growth chamber with controlled conditions at 21°C under long-day conditions (16-h light/8-h dark) with a light intensity of 120-150 µmol m^{-2}. The water was replaced after incubation with 2 mL of deionised water. Electrolyte leakage was measured with Pocket Water Quality Meters (LAQUAtwin-EC-33; Horiba) calibrated at 1.41 mS/cm. Around 100 µL of the sample was used to measure conductivity at the indicated time points. ANOVA (p-value ≤ 0.05) was used for identifying significant factors. Tukey-HSD-Test ($p \leq 0.05$) was used to determine differences between treatment and lines. A detailed statistical summary is available on GitHub: https://github.com/chhilla/HR_gh.

Bacterial growth assay

Pseudomonas syringae pv. tomato (*Pst*) strain DC3000 carrying pVSP61 empty vector or AvrRps4 and *Pst* DC3000 *hrcC*$^{-}$ was grown on selective King's B (KB) medium plates. Bacteria were harvested from the plates, resuspended in infiltration buffer (10 mM $MgCl_2$), and the concentration was adjusted to an optical density of 0.001 at 600 nm [OD_{600}=0.001, representing ~5×10^5 colony-forming units (CFU) mL^{-1}]. Bacteria were infiltrated into abaxial surfaces of 5-week-old Arabidopsis leaves with a 1 mL needleless syringe. For quantification, leaf samples were harvested with a 6 mm diameter cork borer (Z165220; Merck-Sigma-Aldrich), resulting in leaf discs with an area of 0.283 cm^2. Two leaf discs per leaf were harvested as a single sample. For each condition, four samples were collected immediately after infiltration as 'day 0' samples to ensure no significant difference introduced by unequal infiltrations, and six samples were collected at 3 dpi as 'day 3' samples to compare the bacterial growth between different genotypes, conditions, and treatments. For 'day 0',

samples were ground in 200 µL of infiltration buffer and spotted (10 µL per spot) on selective KB medium agar plates to grow for 48 h at 28 °C. For 'day 3', samples were ground in 200 µL of infiltration buffer, serially diluted (5, 50, 500, 5000, and 50 000 times), and spotted (6 µL per spot) on selective KB medium agar plates to grow for 48 h at 28 °C. The number of colonies (CFU per drop) was monitored, and bacterial growth was represented as CFU cm^{-2} of leaf tissue. All results are plotted using ggplot2 in R[49], ANOVA (p-value ≤ 0.05) was used for identifying significant factors. Tukey-HSD-Test (p-value ≤ 0.05) was used to determine differences between treatment and lines. A detailed statistical summary is available on GitHub: https://github.com/chhilla/HR_gh.

Lesion diameter measurement

B. cinerea strain B05.10 was grown as described previously[50] and used for inoculations as described by[51]. Arabidopsis wild type and mutant plants were droplet inoculated with *B. cinerea* at 2.5×10^5 spores/mL in 5 µL of 6 g/L potato dextrose broth, and lesion diameter was measured after 72-96 h. ANOVA (p-value ≤ 0.05) was used for identifying significant factors. Tukey-HSD-Test (p-value ≤ 0.05) was used to determine differences between treatment and lines. A detailed statistical summary is available on GitHub: https://github.com/chhilla/HR_gh.

ROS burst assay

Leaf discs (6 mm diameter) were collected from 5-week-old plants using a cork borer and placed abaxial side down in 96-well plates containing 200 µL of deionized water. Plates were incubated overnight in the dark. The following day, 200 µL of a reaction mixture containing 20 mM luminol (Sigma-Aldrich, A8511), 0.02 mg mL^{-1} horseradish peroxidase (Sigma-Aldrich, P6782), and 100 nM flg22 was added to each well. Reactive oxygen species (ROS) production was quantified using TECAN microplate reader. ANOVA (p-value ≤ 0.05) was used for identifying

significant factors. Tukey-HSD-Test (p-value ≤ 0.05) was used to determine differences between treatment and lines. A detailed statistical summary is available on GitHub: https://github.com/chhilla/HR_gh.

Reverse transcription-quantitative PCR (RT-qPCR) for measuring relative gene expression

For gene expression analysis, RNA was isolated from 5-week-old Arabidopsis leaves and used for subsequent RT–qPCR analysis. RNA was extracted with a VeZol-pure total RNA isolation Kit (RC202-01; Vazyme) and treated with RNase-free DNase (4716728001; Merck-Roche). Reverse transcription was carried out using HiScript III all-in-one RT SuperMix (R333-01; Vazyme). qPCR was performed using a CFX96 Touch™ Real-Time PCR Detection System. Primers for qPCR analysis of *NUDT7* are (F:5'-CTTGCAAGCTAAGTGGATGC-3'; R: 5'-GCGATACTTTAAGGCGCTTG-3')[12]. The elongation factor 1α (EF1α) primers (F: 5'-CAGGCTGATTGTGCTGTTCTTA-3'; R: 5'-GTTGTATCCGACCTTCTTCAGG-3') were used as an internal control. Data were analysed using the double delta Ct method[52]. All results are plotted using ggplot2 in R. A detailed statistical summary is available on GitHub: https://github.com/chhilla/HR_gh.

RNA-seq raw data processing, alignment, quantification of expression, and data visualization

Pseudomonas fluorescens engineered with a Type III secretion system (Pf0-1 'EtHAn' strains) expressing AvrRps4 and AvrRps4KRVY135-138AAAA was infiltrated in 5- to 6-week-old *cbp60g sard1* double mutant *and* wild-type (Col-0) Arabidopsis leaves using a 1 mL needleless syringe. For RNA-seq analysis, two leaves per plant were collected at 4 hours post infiltration (hpi) as one biological replicate. Untreated samples were included as controls. Total RNA was extracted from three biological replicates using the Zymo RNA extraction kit.

The RNA sample was sequenced by Novogene. Raw reads were trimmed into 390 bp clean reads by the Novogene bioinformatics service. At least 12 million paired-end clean reads for each sample were provided by Novogene for RNA-seq analysis. All reads passed FastQC before the following analyses. All clean reads were mapped to a comprehensive Reference Transcript Dataset for Arabidopsis Quantification of Alternatively Spliced Isoforms (AtRTD2_QUASI) containing 82,190 non-redundant transcripts from 34,212 genes via Galaxy and Salmon tools[53,54]. The estimated gene transcript counts were used for differential gene expression analysis and statistical analysis with the 3D RNA-seq software[55]. The low-expressed transcripts were filtered if they did not meet the criteria of ≥3 samples with ≥1 count per million reads. The batch effects between three biological replicates were removed to reduce artificial variance with the RUVSeq method[56]. The expression data were normalised across samples with the TMM (weighted trimmed mean of M-values)[57]. The significance of expression changes in the contrasting groups 'Col-0_kv vs. Col-0_un, groups 'Col-0_a4 vs. Col-0_un', '*gh*_kv vs. *gh*_un' and '*gh*_a4 vs. *gh*_un' were determined by the limma-voom method[58,59]. A gene was defined as a significant differentially expressed gene (DEG) if it had a Benjamini–Hochberg adjusted *p*-value <0.01 and log2[fold change (FC)] ≥ 1 (upregulated) or log2[fold change (FC)] ≤ −1 (downregulated). The GO term analysis was analysed with g:Profiler[60]. Enrichment analysis of transcription factor motifs in the promoters of genes of interest was performed using the AME tool from the MEME Suite[61,62].

Quantification and statistical analysis

All quantitative and statistical analyses were performed using R (version 4.3.1). Data visualization, including boxplots and bar plots, was carried out using the ggplot2 package. Details of the statistical tests applied and

significance thresholds are provided in the corresponding figure legends. RNA-sequencing data were processed and analyzed as described in the RNA-seq analysis section above.

Supplementary Information

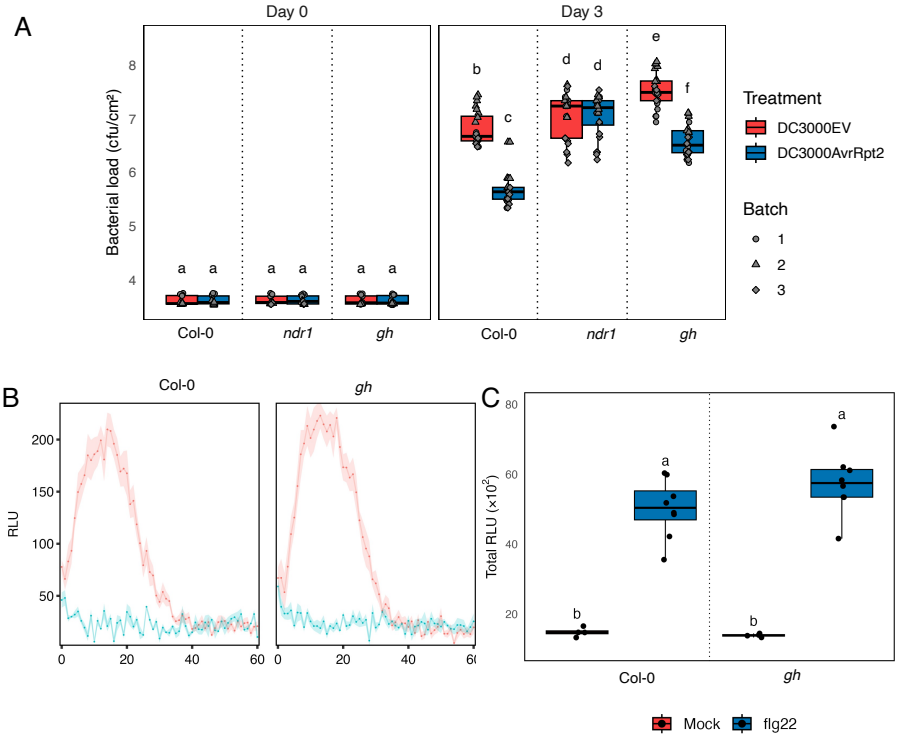

Figure S1. Contribution of CBP60g and SARD1 in PTI and ETI. A. Leaves of Col-0 and the indicated mutant genotypes, *non-race specific disease resistance 1* (*ndr1*) and *cbp60g sard1* (*gh*) were infiltrated with *Pseudomonas syringae* pv. *tomato* DC3000 carrying either an empty vector (EV) or AvrRpt2. Bacterial growth was quantified as colony-forming units (CFU) at 0- and 3-days post-inoculation (dpi). Each data point

represents two pooled leaves from a single plant. Black lines indicate mean values of technical replicates. Statistical differences are indicated by different letters (Tukey's honestly significant difference [HSD] test, p ≤ 0.05). B. Col-0 and *gh* were treated with mock or flg22 and ROS burst is measured. Statistical differences are denoted by different letters (Tukey's HSD test, p ≤ 0.05). C. Total RLU counts in Col-0 and *gh* plants. Statistical differences are denoted by different letters (Tukey's HSD test, $p \leq 0.05$).

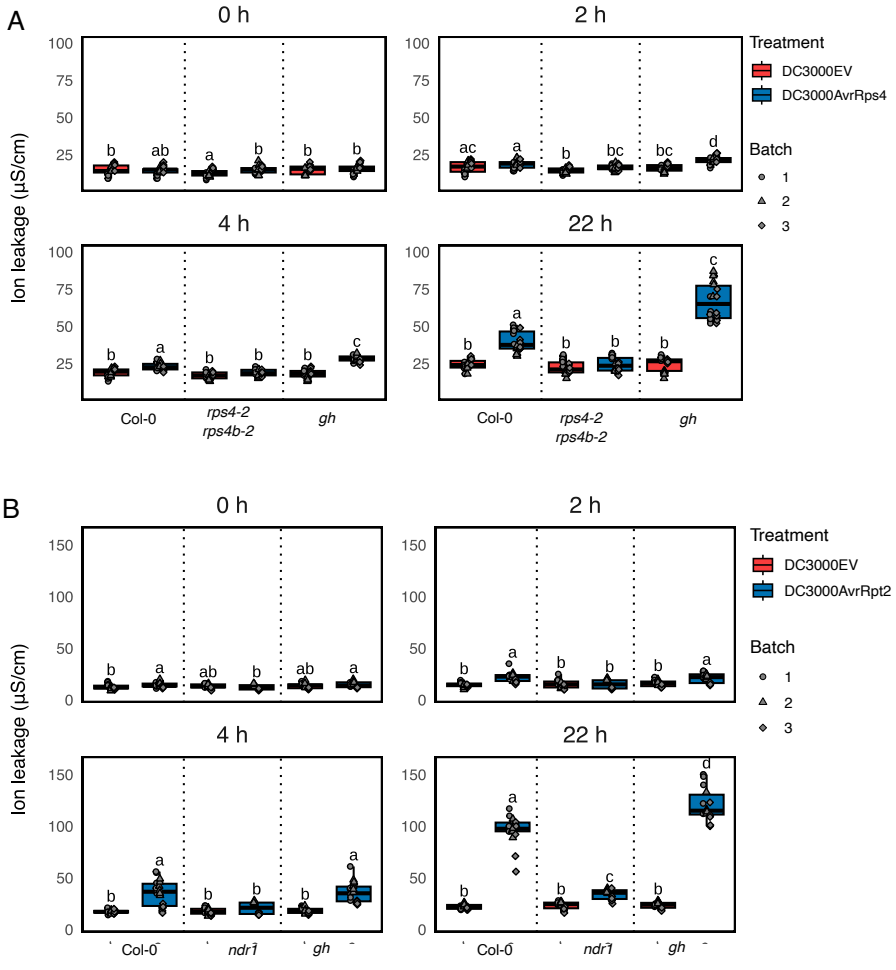

Figure S2. Loss of CBP60g and SARD1 enhances ETIAvrRps4-induced HR. A-B. Ion leakage in indicated mutants infiltrated with *Pseudomonas syringae* DC3000 (empty vector or AvrRps4) and (empty vector or AvrRpt2) measured at interval of 0-22 h post-infiltration. Mutants shown the mutants analysed were *rps4-2 rps4b-2* and *gh* in (A), and *non-ndr1* and *gh* in (B). Different letters indicate statistical significance (Tukey's HSD test, $p \leq 0.05$).

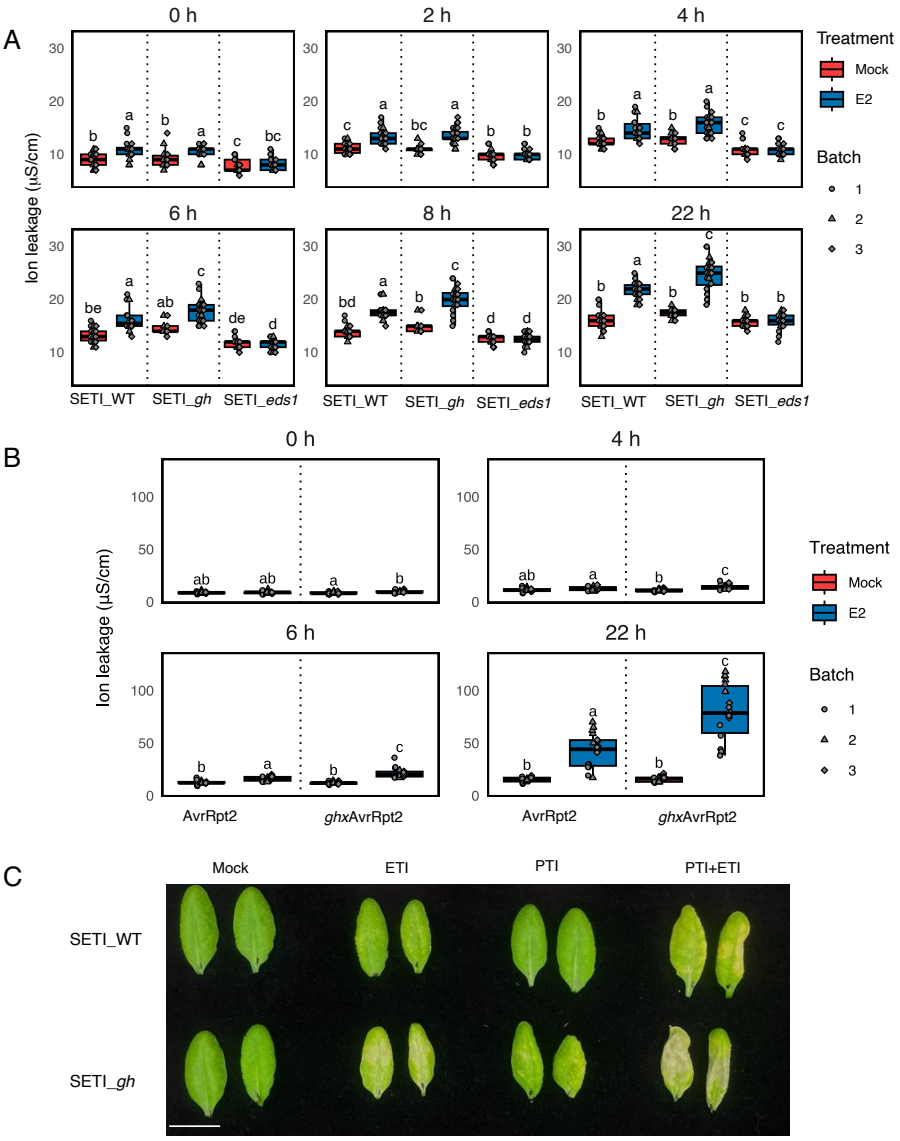

Figure S3. Loss of CBP60g and SARD1 enhances ETI-induced hypersensitive response (HR). A-B. Ion leakage measurements of SETI_WT, SETI_*gh* and SETI_*eds1* infiltrated with mock or estradiol (E2) at the specified time points. Different letters indicate statistically significant differences (Tukey's HSD test, $p \leq 0.05$). C. HR phenotypes of SETI_WT

and SETI_*gh* plants infiltrated with mock, E2 (ETI), DC3000 *hrcC*⁻ (PTI), or PTI+ETI treatments, photographed 3 days post-infiltration. Scale bar = 1 cm.

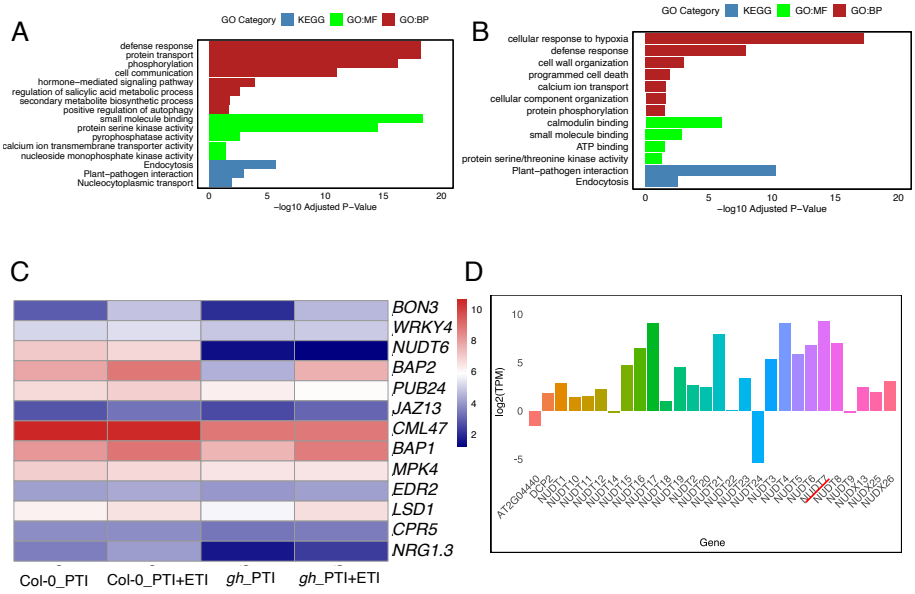

Figure S4. Negative regulation of immune components by CBP60g and SARD1. A-B. GO enrichment analysis of clusters 6 and 10 using g:Profiler, categorized into biological process (GO:BP), cellular component (GO:KEGG), and molecular function (GO:MF) terms (FDR ≤ 0.05, Benjamini–Hochberg correction). C. Heatmap showing expression (Log2TPM) of representative negative immune regulators in WT and *cbp60g sard1* (*gh*) during (PTI) and PTI+ETI. D. Expression profiles of NUDT family members following PTI+ETI treatment. Nudix7 is highlighted with red line.

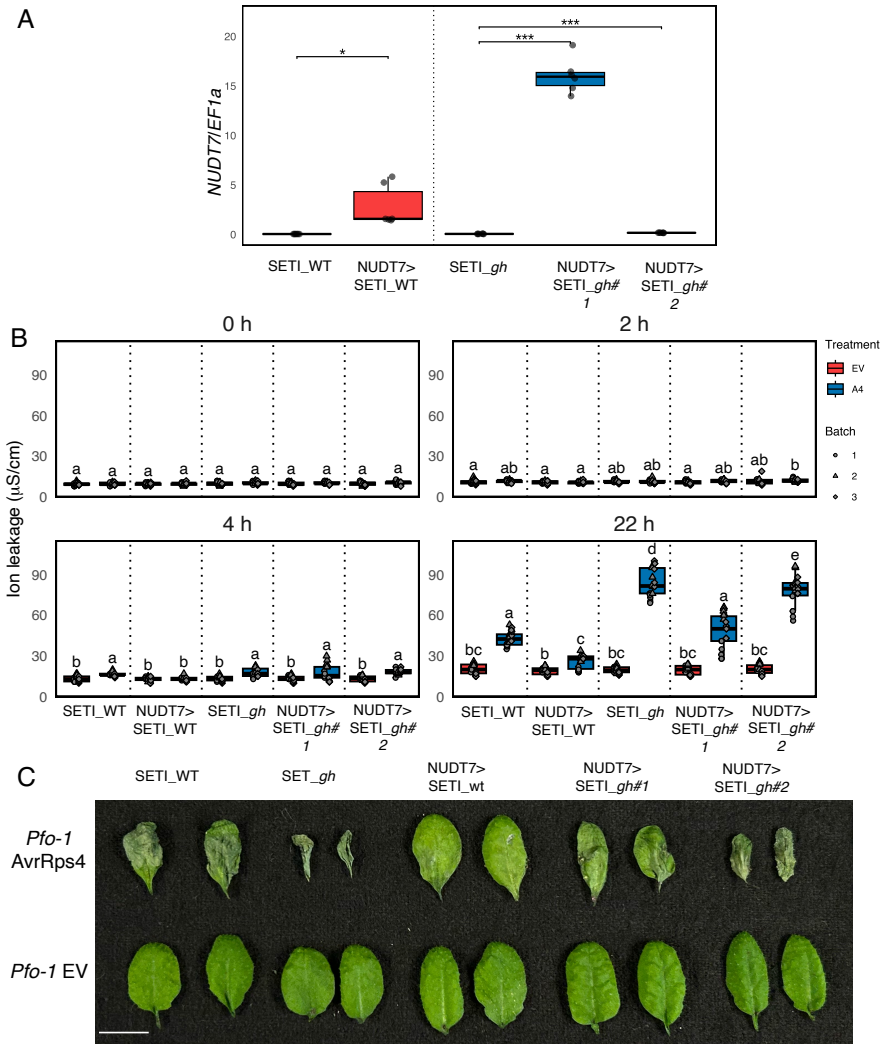

Figure S5. NUDT7 overexpression cannot fully rescue enhanced HR in *cbp60g sard1*. A. Leaves from Five-week-old plants of SETI_WT, SETI_*gh* along with the overexpression lines of NUDT7 in SETI_WT and SETI_*gh* background were harvested for RNA extraction and qPCR. *NUDT7* expression levels are shown relative to *EF1α.* Scale bar = 1 cm. Asterisk indicate significant difference (t-test, $p \leq 0.05$). (#1 and #2 independent lines). B. Ion leakage in indicated mutants infiltrated with

Pseudomonas syringae DC3000 (empty vector or AvrRps4) measured at 0-22 h post-infiltration. Different letters indicate statistical significance (Tukey's HSD test, $p \leq 0.05$). C. HR phenotypes of indicated genotypes infiltrated with *Pf0-1* carrying empty vector or AvrRps4 at 3 days post-infiltration.

Supplemental tables can be accessed online at (https://doi.org/10.1101/2025.06.28.662111).

References

1. Yates, P.L. (1946). Food and agriculture organization of the united nations. Journal of Farm Economics *28*, 54. 10.2307/1232585.

2. Ngou, B.P.M., Jones, J.D.G., and Ding, P. (2022). Plant immune networks. Trends Plant Sci. *27*, 255–273. 10.1016/j.tplants.2021.08.012.

3. Ngou, B.P.M., Ding, P., and Jones, J.D.G. (2022). Thirty years of resistance: Zig-zag through the plant immune system. Plant Cell *34*, 1447–1478. 10.1093/plcell/koac041.

4. Tsuda, K., and Somssich, I.E. (2015). Transcriptional networks in plant immunity. New Phytol. *206*, 932–947. 10.1111/nph.13286.

5. Köster, P., DeFalco, T.A., and Zipfel, C. (2022). Ca2+ signals in plant immunity. EMBO J. *41*, e110741. 10.15252/embj.2022110741.

6. Jiang, Y., and Ding, P. (2023). Calcium signaling in plant immunity: a spatiotemporally controlled symphony. Trends Plant Sci. *28*, 74–89. 10.1016/j.tplants.2022.11.001.

7. Ding, P., and Redkar, A. (2018). Pathogens suppress host transcription factors for rampant proliferation. Trends Plant Sci. *23*, 950–953. 10.1016/j.tplants.2018.08.010.

8. Zhang, Y., Xu, S., Ding, P., Wang, D., Cheng, Y.T., He, J., Gao, M., Xu, F., Li, Y., Zhu, Z., et al. (2010). Control of salicylic acid synthesis and systemic acquired resistance by two members of a

plant-specific family of transcription factors. Proc Natl Acad Sci USA *107*, 18220–18225. 10.1073/pnas.1005225107.

9. Wang, L., Tsuda, K., Truman, W., Sato, M., Nguyen, L.V., Katagiri, F., and Glazebrook, J. (2011). CBP60g and SARD1 play partially redundant critical roles in salicylic acid signaling. Plant J. *67*, 1029–1041. 10.1111/j.1365-313X.2011.04655.x.

10. Truman, W., and Glazebrook, J. (2012). Co-expression analysis identifies putative targets for CBP60g and SARD1 regulation. BMC Plant Biol. *12*, 216. 10.1186/1471-2229-12-216.

11. Truman, W., Sreekanta, S., Lu, Y., Bethke, G., Tsuda, K., Katagiri, F., and Glazebrook, J. (2013). The CALMODULIN-BINDING PROTEIN60 family includes both negative and positive regulators of plant immunity. Plant Physiol. *163*, 1741–1751. 10.1104/pp.113.227108.

12. Sun, T., Zhang, Y., Li, Y., Zhang, Q., Ding, Y., and Zhang, Y. (2015). ChIP-seq reveals broad roles of SARD1 and CBP60g in regulating plant immunity. Nat. Commun. *6*, 10159. 10.1038/ncomms10159.

13. Thordal-Christensen, H. (2020). A holistic view on plant effector-triggered immunity presented as an iceberg model. Cell. Mol. Life Sci. *77*, 3963–3976. 10.1007/s00018-020-03515-w.

14. Balint-Kurti, P. (2019). The plant hypersensitive response: concepts, control and consequences. Mol. Plant Pathol. *20*, 1163–1178. 10.1111/mpp.12821.

15. Künstler, A., Bacsó, R., Gullner, G., Hafez, Y.M., and Király, L. (2016). Staying alive – is cell death dispensable for plant disease resistance during the hypersensitive response? Physiological and Molecular Plant Pathology *93*, 75–84. 10.1016/j.pmpp.2016.01.003.

16. Yu, G.X., Braun, E., and Wise, R.P. (2001). Rds and Rih mediate hypersensitive cell death independent of gene-for-gene resistance to the oat crown rust pathogen Puccinia coronata f. sp. avenae. Mol. Plant Microbe Interact. *14*, 1376–1383. 10.1094/MPMI.2001.14.12.1376.

17. Coll, N.S., Epple, P., and Dangl, J.L. (2011). Programmed cell death in the plant immune system. Cell Death Differ. *18*, 1247–1256. 10.1038/cdd.2011.37.

18. Coll, N.S., Vercammen, D., Smidler, A., Clover, C., Van Breusegem, F., Dangl, J.L., and Epple, P. (2010). Arabidopsis type I metacaspases control cell death. Science *330*, 1393–1397. 10.1126/science.1194980.

19. Yu, I.C., Parker, J., and Bent, A.F. (1998). Gene-for-gene disease resistance without the hypersensitive response in Arabidopsis dnd1 mutant. Proc Natl Acad Sci USA *95*, 7819–7824. 10.1073/pnas.95.13.7819.

20. Balagué, C., Lin, B., Alcon, C., Flottes, G., Malmström, S., Köhler, C., Neuhaus, G., Pelletier, G., Gaymard, F., and Roby, D. (2003). HLM1, an essential signaling component in the hypersensitive response, is a member of the cyclic nucleotide-gated channel ion channel family. Plant Cell *15*, 365–379. 10.1105/tpc.006999.

21. Lorrain, S., Vailleau, F., Balagué, C., and Roby, D. (2003). Lesion mimic mutants: keys for deciphering cell death and defense pathways in plants? Trends Plant Sci. *8*, 263–271. 10.1016/S1360-1385(03)00108-0.

22. Greenberg, J.T., and Yao, N. (2004). The role and regulation of programmed cell death in plant-pathogen interactions. Cell. Microbiol. *6*, 201–211. 10.1111/j.1462-5822.2004.00361.x.

23. Narusaka, M., Shirasu, K., Noutoshi, Y., Kubo, Y., Shiraishi, T., Iwabuchi, M., and Narusaka, Y. (2009). RRS1 and RPS4 provide a dual Resistance-gene system against fungal and bacterial pathogens. Plant J. *60*, 218–226. 10.1111/j.1365-313X.2009.03949.x.

24. Saucet, S.B., Ma, Y., Sarris, P.F., Furzer, O.J., Sohn, K.H., and Jones, J.D.G. (2015). Two linked pairs of Arabidopsis TNL resistance genes independently confer recognition of bacterial effector AvrRps4. Nat. Commun. *6*, 6338. 10.1038/ncomms7338.

25. Kunkel, B.N., Bent, A.F., Dahlbeck, D., Innes, R.W., and Staskawicz, B.J. (1993). RPS2, an Arabidopsis disease resistance locus specifying recognition of Pseudomonas syringae strains expressing the avirulence gene avrRpt2. Plant Cell *5*, 865–875. 10.1105/tpc.5.8.865.

26. Axtell, M.J., and Staskawicz, B.J. (2003). Initiation of RPS2-specified disease resistance in Arabidopsis is coupled to the AvrRpt2-directed elimination of RIN4. Cell *112*, 369–377. 10.1016/s0092-8674(03)00036-9.

27. Huang, W., Wang, Y., Li, X., and Zhang, Y. (2020). Biosynthesis and Regulation of Salicylic Acid and N-Hydroxypipecolic Acid in Plant Immunity. Mol. Plant *13*, 31–41. 10.1016/j.molp.2019.12.008.

28. Thomas, W.J., Thireault, C.A., Kimbrel, J.A., and Chang, J.H. (2009). Recombineering and stable integration of the Pseudomonas syringae pv. syringae 61 hrp/hrc cluster into the genome of the soil bacterium Pseudomonas fluorescens Pf0-1. Plant J. *60*, 919–928. 10.1111/j.1365-313X.2009.03998.x.

29. Sohn, K.H., Hughes, R.K., Piquerez, S.J., Jones, J.D.G., and Banfield, M.J. (2012). Distinct regions of the Pseudomonas syringae coiled-coil effector AvrRps4 are required for activation of immunity. Proc Natl Acad Sci USA *109*, 16371–16376. 10.1073/pnas.1212332109.

30. McNellis, T.W., Mudgett, M.B., Li, K., Aoyama, T., Horvath, D., Chua, N.H., and Staskawicz, B.J. (1998). Glucocorticoid-inducible expression of a bacterial avirulence gene in transgenic Arabidopsis induces hypersensitive cell death. Plant J. *14*, 247–257. 10.1046/j.1365-313x.1998.00106.x.

31. Ngou, B.P.M., Ahn, H.-K., Ding, P., Redkar, A., Brown, H., Ma, Y., Youles, M., Tomlinson, L., and Jones, J.D.G. (2020). Estradiol-inducible AvrRps4 expression reveals distinct properties of TIR-NLR-mediated effector-triggered immunity. J. Exp. Bot. *71*, 2186–2197. 10.1093/jxb/erz571.

32. Derbyshire, M.C., and Raffaele, S. (2023). Till death do us pair: Co-evolution of plant-necrotroph interactions. Curr. Opin. Plant Biol. *76*, 102457. 10.1016/j.pbi.2023.102457.

33. Lai, Z., and Mengiste, T. (2013). Genetic and cellular mechanisms regulating plant responses to necrotrophic pathogens. Curr. Opin. Plant Biol. *16*, 505–512. 10.1016/j.pbi.2013.06.014.

34. Radojičić, A., Li, X., and Zhang, Y. (2018). Salicylic Acid: A Double-Edged Sword for Programed Cell Death in Plants. Front. Plant Sci. *9*, 1133. 10.3389/fpls.2018.01133.

35. Ding, P., Ngou, B.P.M., Furzer, O.J., Sakai, T., Shrestha, R.K., MacLean, D., and Jones, J.D.G. (2020). High-resolution expression profiling of selected gene sets during plant immune activation. Plant Biotechnol. J. *18*, 1610–1619. 10.1111/pbi.13327.

36. Sohn, K.H., Segonzac, C., Rallapalli, G., Sarris, P.F., Woo, J.Y., Williams, S.J., Newman, T.E., Paek, K.H., Kobe, B., and Jones, J.D.G. (2014). The nuclear immune receptor RPS4 is required for RRS1SLH1-dependent constitutive defense activation in Arabidopsis thaliana. PLoS Genet. *10*, e1004655. 10.1371/journal.pgen.1004655.

37. Ngou, B.P.M., Ahn, H.-K., Ding, P., and Jones, J.D.G. (2021). Mutual potentiation of plant immunity by cell-surface and intracellular receptors. Nature *592*, 110–115. 10.1038/s41586-021-03315-7.

38. Sun, T., Liang, W., Zhang, Y., and Li, X. (2018). Negative regulation of resistance protein-mediated immunity by master

transcription factors SARD1 and CBP60g. J. Integr. Plant Biol *60*, 1023–1027. 10.1111/jipb.12698.

39. Kraszewska, E. (2008). The plant Nudix hydrolase family. Acta Biochim. Pol. *55*, 663–671.

40. Bartsch, M., Gobbato, E., Bednarek, P., Debey, S., Schultze, J.L., Bautor, J., and Parker, J.E. (2006). Salicylic acid-independent ENHANCED DISEASE SUSCEPTIBILITY1 signaling in Arabidopsis immunity and cell death is regulated by the monooxygenase FMO1 and the Nudix hydrolase NUDT7. Plant Cell *18*, 1038–1051. 10.1105/tpc.105.039982.

41. Straus, M.R., Rietz, S., Ver Loren van Themaat, E., Bartsch, M., and Parker, J.E. (2010). Salicylic acid antagonism of EDS1-driven cell death is important for immune and oxidative stress responses in Arabidopsis. Plant J. *62*, 628–640. 10.1111/j.1365-313X.2010.04178.x.

42. Wang, H., Lu, Y., Liu, P., Wen, W., Zhang, J., Ge, X., and Xia, Y. (2013). The ammonium/nitrate ratio is an input signal in the temperature-modulated, SNC1-mediated and EDS1-dependent autoimmunity of nudt6-2 nudt7. Plant J. *73*, 262–275. 10.1111/tpj.12032.

43. Yu, D., Song, W., Tan, E.Y.J., Liu, L., Cao, Y., Jirschitzka, J., Li, E., Logemann, E., Xu, C., Huang, S., et al. (2022). TIR domains of plant immune receptors are 2',3'-cAMP/cGMP synthetases mediating cell death. Cell *185*, 2370-2386.e18. 10.1016/j.cell.2022.04.032.

44. Nawrath, C., and Métraux, J.P. (1999). Salicylic acid induction-deficient mutants of Arabidopsis express PR-2 and PR-5 and accumulate high levels of camalexin after pathogen inoculation. Plant Cell *11*, 1393–1404. 10.1105/tpc.11.8.1393.

45. Castel, B., Ngou, P.-M., Cevik, V., Redkar, A., Kim, D.-S., Yang, Y., Ding, P., and Jones, J.D.G. (2019). Diverse NLR immune receptors activate defence via the RPW8-NLR NRG1. New Phytol. *222*, 966–980. 10.1111/nph.15659.

46. Laflamme, B., Dillon, M.M., Martel, A., Almeida, R.N.D., Desveaux, D., and Guttman, D.S. (2020). The pan-genome effector-triggered immunity landscape of a host-pathogen interaction. Science *367*, 763–768. 10.1126/science.aax4079.

47. Falk, A., Feys, B.J., Frost, L.N., Jones, J.D., Daniels, M.J., and Parker, J.E. (1999). EDS1, an essential component of R gene-mediated disease resistance in Arabidopsis has homology to eukaryotic lipases. Proc Natl Acad Sci USA *96*, 3292–3297. 10.1073/pnas.96.6.3292.

48. Ordon, J., Gantner, J., Kemna, J., Schwalgun, L., Reschke, M., Streubel, J., Boch, J., and Stuttmann, J. (2017). Generation of chromosomal deletions in dicotyledonous plants employing a user-friendly genome editing toolkit. Plant J. *89*, 155–168. 10.1111/tpj.13319.

49. Wickham, H. (2016). ggplot2: Elegant Graphics for Data Analysis (Use R!) 2nd ed. (Springer).

50. Stefanato, F.L., Abou-Mansour, E., Buchala, A., Kretschmer, M., Mosbach, A., Hahn, M., Bochet, C.G., Métraux, J.-P., and Schoonbeek, H. (2009). The ABC transporter BcatrB from Botrytis cinerea exports camalexin and is a virulence factor on Arabidopsis thaliana. Plant J. *58*, 499–510. 10.1111/j.1365-313X.2009.03794.x.

51. Schoonbeek, H.-J., Yalcin, H.A., Burns, R., Taylor, R.E., Casey, A., Holt, S., Van den Ackerveken, G., Wells, R., and Ridout, C.J. (2022). Necrosis and ethylene-inducing-like peptide patterns from crop pathogens induce differential responses within seven brassicaceous species. Plant Pathol. *71*, 2004–2016. 10.1111/ppa.13615.

52. Livak, K.J., and Schmittgen, T.D. (2001). Analysis of relative gene expression data using real-time quantitative PCR and the 2(-Delta Delta C(T)) Method. Methods *25*, 402–408. 10.1006/meth.2001.1262.

53. Zhang, R., Kuo, R., Coulter, M., Calixto, C.P.G., Entizne, J.C., Guo, W., Marquez, Y., Milne, L., Riegler, S., Matsui, A., et al. (2022). A high-resolution single-molecule sequencing-based Arabidopsis transcriptome using novel methods of Iso-seq analysis. Genome Biol. *23*, 149. 10.1186/s13059-022-02711-0.

54. Bray, N.L., Pimentel, H., Melsted, P., and Pachter, L. (2016). Near-optimal probabilistic RNA-seq quantification. Nat. Biotechnol. *34*, 525–527. 10.1038/nbt.3519.

55. Guo, W., Tzioutziou, N.A., Stephen, G., Milne, I., Calixto, C.P., Waugh, R., Brown, J.W.S., and Zhang, R. (2021). 3D RNA-seq: a

powerful and flexible tool for rapid and accurate differential expression and alternative splicing analysis of RNA-seq data for biologists. RNA Biol. *18*, 1574–1587. 10.1080/15476286.2020.1858253.

56. Risso, D., Ngai, J., Speed, T.P., and Dudoit, S. (2014). Normalization of RNA-seq data using factor analysis of control genes or samples. Nat. Biotechnol. *32*, 896–902. 10.1038/nbt.2931.

57. Robinson, M.D., and Oshlack, A. (2010). A scaling normalization method for differential expression analysis of RNA-seq data. Genome Biol. *11*, R25. 10.1186/gb-2010-11-3-r25.

58. Law, C.W., Chen, Y., Shi, W., and Smyth, G.K. (2014). voom: Precision weights unlock linear model analysis tools for RNA-seq read counts. Genome Biol. *15*, R29. 10.1186/gb-2014-15-2-r29.

59. Ritchie, M.E., Phipson, B., Wu, D., Hu, Y., Law, C.W., Shi, W., and Smyth, G.K. (2015). limma powers differential expression analyses for RNA-sequencing and microarray studies. Nucleic Acids Res. *43*, e47. 10.1093/nar/gkv007.

60. Kolberg, L., Raudvere, U., Kuzmin, I., Adler, P., Vilo, J., and Peterson, H. (2023). g:Profiler-interoperable web service for functional enrichment analysis and gene identifier mapping (2023 update). Nucleic Acids Res. *51*, W207–W212. 10.1093/nar/gkad347.

61. Bailey, T.L., Johnson, J., Grant, C.E., and Noble, W.S. (2015). The MEME Suite. Nucleic Acids Res. *43*, W39-49. 10.1093/nar/gkv416.

62. McLeay, R.C., and Bailey, T.L. (2010). Motif Enrichment Analysis: a unified framework and an evaluation on ChIP data. BMC Bioinformatics *11*, 165. 10.1186/1471-2105-11-165.